Large-Scale Atmospheric Forcing by Southeast Pacific Boundary Layer Clouds: A Regional Model Study*

YUQING WANG, SHANG-PING XIE,+ BIN WANG,+ AND HAIMING XU

International Pacific Research Center, School of Ocean and Earth Science and Technology, University of Hawaii at Manoa, Honolulu, Hawaii

(Manuscript received 22 April 2004, in final form 13 August 2004)

ABSTRACT

A regional model is used to study the radiative effect of boundary layer clouds over the southeast Pacific on large-scale atmosphere circulation during August–October 1999. With the standard settings, the model simulates reasonably well the large-scale circulation over the eastern Pacific, precipitation in the intertropical convergence zone (ITCZ) north of the equator, and marine boundary layer stratocumulus clouds to the south. In a sensitivity experiment with the radiative effect of liquid clouds south of the equator over the eastern Pacific artificially removed, boundary layer clouds south of the equator almost disappear and precipitation in the ITCZ is reduced by 15%–20%, indicating that the stratocumulus clouds over the southeast Pacific have both local and cross-equatorial effects.

Examination of the differences between the control and sensitivity experiments indicates that clouds exert a net diabatic cooling in the inversion layer. In response to this cloud-induced cooling, an in situ anomalous high pressure system develops in the boundary layer and an anomalous shallow meridional circulation develops in the lower troposphere over the equatorial eastern Pacific. At the lower branch of this shallow circulation, anomalous boundary layer southerlies blow from the boundary layer high toward the northern ITCZ where the air ascends. An anomalous returning flow (northerly) just above the cloud layer closes the shallow circulation.

This low-level anomalous shallow circulation enhances the subsidence over the southeast Pacific above the cloud layer, helping to maintain boundary layer clouds and temperature inversion there. Meanwhile, the strengthened cross-equatorial flow near the surface enhances moisture convergence and convection in the ITCZ north of the equator. This in turn strengthens the local, deep Hadley circulation and hence the large-scale subsidence and boundary layer clouds over the southeast Pacific. This positive feedback therefore enhances the interhemispheric climate asymmetry over the tropical eastern Pacific.

1. Introduction

Marine boundary layer (MBL) clouds cover on an average one-third of the earth's oceans (Klein and Hartmann 1993). The high albedo (30%–40%) of MBL clouds compared to the underlying ocean surface (~6%) gives rise to the large deficits in the absorbed solar radiative fluxes both at the top of the atmosphere and at the underlying ocean surface, while their low altitude prevents significant compensation in thermal emission (Randall et al. 1984; Norris 1998). The MBL clouds can also modify the boundary layer structure and the fluxes both at the sea surface and across the temperature inversion through condensation and precipitation, generation of turbulence, and radiative transfer (Moeng 2000; Yuter et al. 2000; Stevens et al. 2003). Despite their climatic importance, these low clouds are poorly simulated in many state-of-the-art global atmospheric general circulation models (GCMs; Bretherton et al. 2004).

Over the southeast Pacific off South America, an extensive MBL stratocumulus (SCu) cloud deck reflects incoming solar radiation and reduces the local sea surface temperature (SST), which in turn enhances the SCu clouds by strengthening the capping temperature inversion. This positive feedback and its potential contribution to realistic simulations of the intertropical convergence zone (ITCZ) over the eastern Pacific have been demonstrated by coupled general circulation

* International Pacific Research Center Contribution Number IPRC 295 and School of Ocean and Earth Science and Technology Contribution Number 6488.

+ Additional affiliation: Department of Meteorology, University of Hawaii at Manoa, Honolulu, Hawaii.

Corresponding author address: Dr. Yuqing Wang, IPRC/SOEST, University of Hawaii at Manoa, 2525 Correa Road, Honolulu, HI 96822.
E-mail: yqwang@soest.hawaii.edu

model (CGCM) experiments (Philander et al. 1996; Ma et al. 1996; Bachiochi and Krishnamurti 2000). These studies show that the radiative cooling due to the presence of MBL clouds strengthens the SST gradients in both the meridional and zonal directions, enhancing the trade winds. The subsequent interaction of SST and the trade winds takes the form of westward-propagating coupled waves (Xie 1996), causing a basin-wide adjustment in ocean and atmosphere circulation (Yu and Mechoso 1999; Gordon et al. 2000; Xie and Saito 2001).

MBL clouds also have a net radiative cooling effect on the lower troposphere. With steady-state linear primitive equation models, Nigam (1997) and Bergman and Hendon (2000) found that this radiative atmospheric cooling is important for seasonal variations in cross-equatorial surface winds over the tropical eastern Pacific. Nigam (1997) further proposed a positive feedback in which the longwave radiative cooling of the MBL due to the SCu cloud deck over the tropical southeastern Pacific generates southerly surface winds, which in turn enhance SCu clouds by increasing the meridional cold advection and latent heat flux. Linear steady-state models, however, can only elucidate the atmospheric circulation responses to the specified cloud radiative cooling but not the response and feedback of MBL clouds and ITCZ to the cloud-induced circulation changes. Therefore, further studies with more realistic models are required to investigate this positive feedback and to understand its potential effect on the eastern Pacific climate.

The objective of this work is to further study this positive feedback over the tropical eastern Pacific with a regional climate model developed at University of Hawaii's International Pacific Research Center (hereafter IPRC–RegCM). The use of a regional atmospheric model is justified by the finding of Bergman and Hendon (2000), who concluded that cloud–radiative forcing tends to mostly influence regional circulations. More importantly, the IPRC–RegCM with the use of a relatively large model domain allows interaction among atmospheric circulation, MBL clouds, and ITCZ convection, as described in Wang et al. (2004a,b). In our study, the observed SST distribution is used as the lower boundary condition to exclude the positive feedback between MBL clouds and the underlying SST and thus to focus on the positive feedback between MBL clouds and the atmospheric circulation. We will show that MBL clouds have both local and remote effects and enhance the interhemispheric climate asymmetry over the tropical eastern Pacific through a positive cloud-circulation feedback, as hypothesized by Nigam (1997).

The rest of the paper is organized as follows. The next section describes the numerical model and design of numerical experiments. Section 3 discusses the simulated boundary layer clouds and their local effect on the boundary layer structure over the southeast Pacific off South America. Section 4 examines the large-scale atmospheric forcing induced by boundary layer clouds over the southeast Pacific. Main conclusions are drawn in the last section.

2. The model and experimental design

a. The IPRC–RegCM (version 1.2)

The model used in this study is the regional climate model, IPRC–RegCM, developed at the International Pacific Research Center. A detailed description of the IPRC–RegCM (version 1.1) and its performance in simulating regional climate over East Asia can be found in Wang et al. (2003). The model has also been used in modeling the regional climate over the eastern Pacific, including the response of the atmosphere to the Pacific tropical instability ocean waves (Small et al. 2003), simulation of boundary layer clouds over the southeast Pacific (Wang et al. 2004a,b), and the effect of the Andean mountains on eastern Pacific climate (Xu et al. 2004).

The model uses hydrostatic primitive equations in spherical coordinates with σ as the vertical coordinate. The model equations are solved with a fourth-order conservative finite-difference scheme on an unstaggered longitude/latitude grid system and a leapfrog scheme with intermittent use of an Euler backward scheme for time integration. The model has 30 levels in the vertical with high resolution in the planetary boundary layer (11 levels below 800 hPa). The model physics include the cloud microphysics scheme of Wang (1999, 2001); a mass flux scheme for subgrid shallow convection, midlevel convection, and deep convection developed by Tiedtke (1989) and modified by Nordeng (1995) and Gregory et al. (2000); the radiation package developed by Edwards and Slingo (1996) and further improved later by Sun and Rikus (1999); the Biosphere–Atmosphere Transfer Scheme (BATS) developed by Dickinson et al. (1993) for land surface processes; a modified Monin–Obukhov similarity scheme for flux calculations at the ocean surface (Wang 2002); and a nonlocal E–ε turbulence closure scheme for subgrid-scale vertical mixing (Langland and Liou 1996), which was modified to include the effect of cloud buoyancy production of turbulence kinetic energy (Wang 1999). Table 1 provides a summary of the physical parameterization schemes used in the IPRC–RegCM version 1.2.

The modified mass flux scheme uses a CAPE (convective available potential energy) closure and considers the organized entrainment/detrainment based on a simple cloud plume model for deep convection (Nordeng 1995; Gregory et al. 2000). The cloud water/ice detrained from cumulus towers is allowed to contribute to grid-scale cloud water/ice, which leads to improved model cloudiness calculation in the IPRC–RegCM (Wang et al. 2003). This feedback of the detained cloud water/ice depends on the environmental relative hu-

TABLE 1. List of physics parameterization schemes used in the IPRC-RegCM (version 1.2). Also included are references and comments where necessary.

Physical process	Scheme	Reference	Comments
Grid-resolved moist processes	Bulk mixed-ice-phase cloud microphysics	Wang (1999, 2001)	Based mainly on Lin et al. (1983), Rutledge and Hobbs (1983), and Reisner et al. (1998).
Subgrid-scale convection	Shallow convection, midlevel convection, and deep convection	Tiedke (1989); Nordeng (1995); Gregory et al. (2000)	With CAPE closure and organized entrainment and detrainment. Coupling between subgrid-scale convection and grid-resolved moist processes via cloud-top detrainment (Wang et al. 2003).
Mixing	Vertical: 1.5-level nonlocal turbulence closure	Langland and Liou (1996)	Modified to include cloud buoyancy production of turbulence (Wang 1999).
	Horizontal: fourth order	Wang et al. (2003)	Deformation and terrain-slope dependent diffusion coefficient.
Surface layer over ocean	Bulk scheme	Fairall et al. (2003)	TOGA COARE v3.0
Radiation	Multiband	Edwards and Slingo (1982); Chou et al. (1998)	Seven bands for longwave, four bands for shortwave, full coupling between cloud microphysics and cloud liquid/ice water extent.
Cloud optical properties	Longwave radiation	Sun and Shine (1994)	
	Shortwave radiation	Slingo and Schrecker (1982); Chou et al. (1998)	With specified cloud droplet number concentration (CDNC) of 100 cm^{-3} over ocean and 300 cm^{-3} over land.
Cloud amount	Semi-empirical scheme	Xu and Randall (1996)	Dependent on relative humidity and cloud liquid/ice water extent.
Land surface processes	Biosphere–Atmosphere Transfer Scheme (BATS)	Dickenson et al. (1993)	Modified algorithm for solving leaf temperature to ensure a convergent iteration of numerical solution (Wang et al. 2003).

midity so that immediate and complete evaporation of detrained cloud water/ice is assumed for relatively dry conditions. Specifically, only the portion ($\overline{q_d}$) of the detrained cloud condensates (q_d) is used to increase the grid scale cloud water mixing ratio

$$\overline{q_d} = \text{Max}\left[0.0, \left(\frac{\text{RH} - \text{RH}_c}{1 - \text{RH}_c}\right) q_d\right], \qquad (1)$$

where RH is the mean relative humidity in a grid box and RH_c is a critical relative humidity below which the detrained cloud condensates evaporate immediately and is set to be 0.8 in our application. Note that the rest of the detrained cloud condensates are assumed to evaporate instantaneously and increase the environmental relative humidity. The partitioning of the detrained cloud condensates between cloud water and cloud ice above the freezing level is a function of temperature given by Rockel et al. (1991) [see Eq. (1) in Wang et al. (2003)].

As indicated in Wang et al. (2004a,b) and McCaa and Bretherton (2004), the simulation of MBL stratocumulus clouds depends strongly on the parameterization of shallow convection in the model. In the IPRC–RegCM, the mass flux scheme of Tiedtke (1989) is used. For a reasonable simulation, Wang et al. (2004a) adjusted the fraction of the cloud ensemble that penetrates into the inversion layer and detrains there into the environment from the default value 0.33–0.23 [β in Eq. (21); Tiedtke (1989)] for shallow convection. This is used in conjunction with the simple Kessler (1969) drizzle parameterization in the cloud microphysics scheme (Wang 1999, 2001), with the threshold cloud water mixing ratio set at 0.4 g kg^{-1} above which effective conversion of cloud water into rainwater (or drizzle) occurs. In this new version of IPRC–RegCM (V1.2) used here, we increased this threshold to 0.5 g kg^{-1} to reduce drizzle from SCu clouds and used the fraction of 0.3 for detrained clouds in the inversion layer. These adjustments in parameters improve the simulation of boundary layer clouds near the coast of South America in the new version of the IPRC–RegCM (see section 3a).

The radiation package includes seven/four bands for longwave/shortwave radiation calculation. We considered a full coupling between the cloud microphysics and the cloud water/ice path used in radiation calculations. The cloud radiative properties are calculated based on Sun and Shine (1994) for longwave radiation, and Slingo and Schrecker (1982) and Chou et al. (1998) for shortwave radiation. Sun and Pethick (2002) found that this is a good combination for marine SCu clouds. Note that because of the lack of information of cloud condensation nuclei, which depends on the size distribution of water-soluble species (sulfates, organics, sea salt, and nitrates) and the degree of solubility and the mixing ratio of individual species within a given size fraction, the cloud droplet number concentration (CDNC) has to be specified in the model. Although the simulated MBL SCu clouds could be very sensitive to this specification (e.g., McCaa and Bretherton 2004), we simply set CDNC to be 100 cm^{-3} over the ocean and 300 cm^{-3} over the land: both are representative for the

interested region (Bretherton et al. 2004). However, more realistic specification of CNDC can be achieved in future studies by incorporating the effect of aerosols and a higher moments cloud microphysics scheme. Cloud amount is diagnosed using the semiempirical cloudiness parameterization scheme developed by Xu and Randall (1996), by which cloud amount is determined by both relative humidity and liquid/ice water content.

Note that in the latest version of the IPRC–RegCM, the third-order upstream advection scheme of Wang (1996) was used for time integration of equations for mixing ratios of water vapor and all hydrometeors, turbulent kinetic energy, and its dissipation rate. This scheme has very weak numerical dissipation, small dispersion error, and better shape-conserving properties compared to the fourth-order centered finite-difference scheme that was used in the previous version of the IPRC–RegCM (Wang 1996).

b. Experimental design

The regional climate model described above is used to study eastern Pacific climate in the boreal fall [August, September, and October (ASO)] in 1999, which was a moderate La Niña. To include convective precipitation in the ITCZ north of the equator, which may have a large-scale control on and be influenced by boundary layer clouds over the southeast Pacific through the meridional Hadley circulation, the model domain is chosen to cover a large portion of the eastern Pacific and the South American continent (35°S–35°N, 150°–30°W). The model uses a horizontal grid spacing of 0.5°, thus including 241 by 141 grid points. The U.S. Geological Survey (USGS) high-resolution topographic dataset (0.0833° × 0.0833°) was used to obtain the model envelope topography (Fig. 1a).

The National Centers for Environmental Prediction–National Center for Atmospheric Research (NCEP–NCAR) reanalysis data available at every 6-h interval with a resolution of 2.5° × 2.5° in the horizontal and 17 pressure levels up to 10 hPa (Kalnay et al. 1996) were used as both initial and lateral boundary conditions for the regional climate model. A one-way nesting was used to update the model time integration in a buffer zone (12 grid points) near the lateral boundaries within which the model prognostic variables were nudged to the reanalysis data (Wang et al. 2003). Since there were no hydrometeor fields from the reanalysis data at the lateral boundaries, mixing ratios of cloud water, rainwater, cloud ice, snow, and graupel were set to be zero at inflow boundaries, while they were advected outward at the outflow boundaries. This outflow boundary condition was also used for both turbulent kinetic energy and its dissipation rate. To minimize edge effects from the lateral boundaries, our analysis will be confined in the interior region within 30°S–30°N, 140°–40°W (Fig. 1a).

Over the ocean, SSTs were obtained from the Reynolds and Smith (1994) weekly SST data with horizontal resolution of 1° × 1°, which were interpolated onto the model grid by a cubic spline interpolation in space and linearly interpolated in time. Over the land, the initial surface soil and canopy temperatures were obtained from the lowest model level with a standard lapse rate of 6.5°C km^{-1}. Initial snow depths were set to be zero, while the soil moisture fields were initialized such that the initial soil moisture depends on the vegetation and soil type defined for each grid cell (Giorgi and Bates 1989).

The model was initialized from 0000 UTC on 29 July and integrated continuously through 31 October 1999. Two experiments were conducted: one with the standard model configuration as described above (CTL), and one that removes the effect of boundary layer clouds on the radiation budget south of the equator over the eastern Pacific by simply setting cloud liquid water to zero there in the radiation budget (NoCLD).

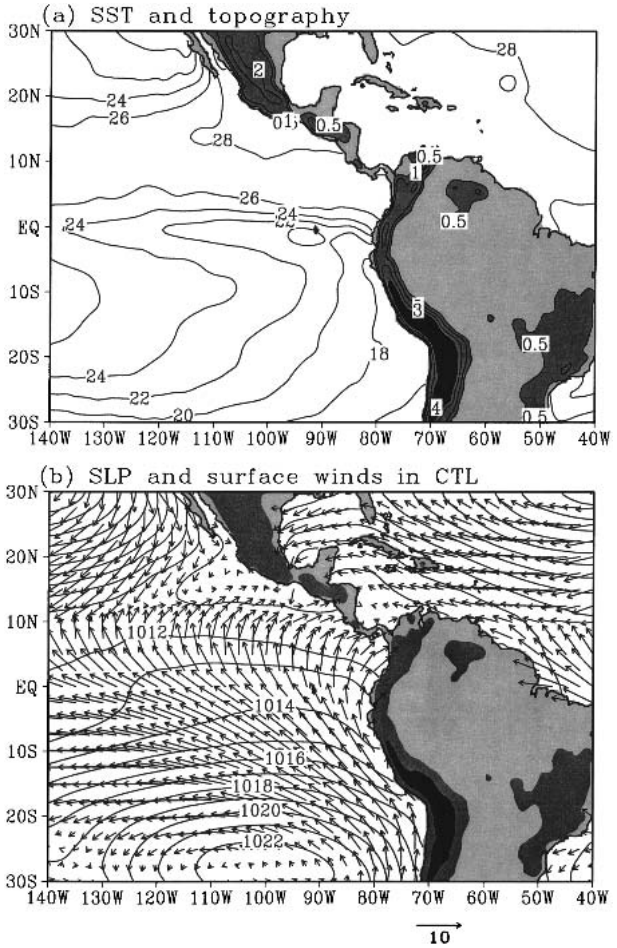

FIG. 1. (a) Interior model domain and topography in km with contours of 0.5, 1, 2, 3, and 4 km (light and heavy shadings show topography higher than 1 and 3 km, respectively) and SST (contours in °C) averaged in ASO 1999. (b) Model mean sea level pressure (contours in hPa) and 10-m height winds (vectors in m s^{-1}) averaged in ASO 1999 from CTL.

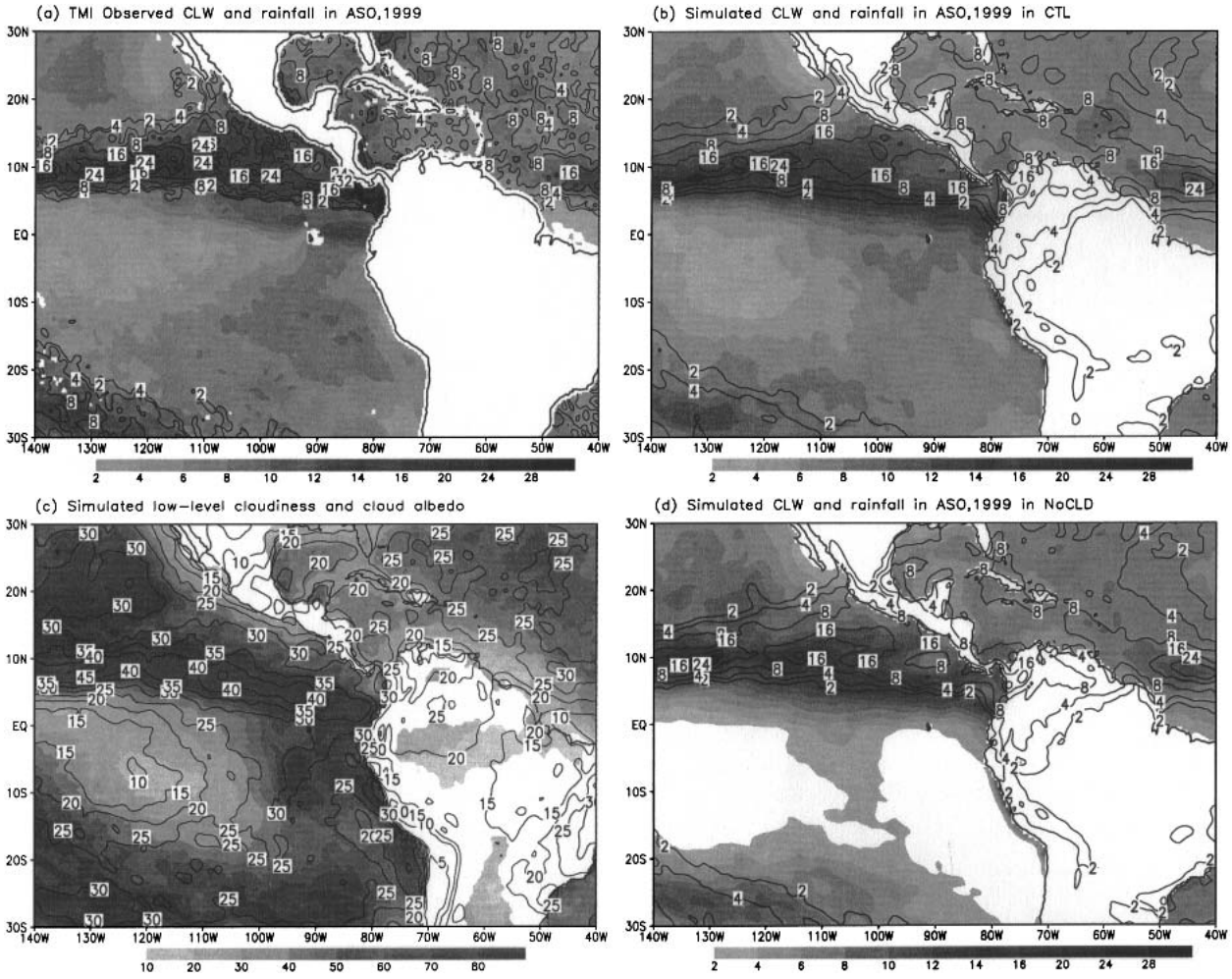

FIG. 2. Column-integrated liquid water content (shaded, 10^{-2} mm) and daily rainfall (contours in 2, 4, 8, 16, 24 mm day^{-1}) averaged in ASO 1999 from (a) TMI observation, (b) simulation in CTL, and (d) simulation in NoCLD. (c) The cloudiness below sigma = 0.7 (shaded, below about 700 hPa over the ocean) and the total cloud albedo (contours) are shown in percentages.

We will show that in CTL the model simulates the boundary layer clouds reasonably well, while in NoCLD marine boundary layer clouds south of the equator are greatly reduced due to the removal of the cloud radiation feedback, which is crucial to formation and maintenance of boundary layer clouds (Moeng and Lenschow 1995). Since the same SST forcing is used in the two experiments, radiative effects of boundary layer clouds over the southeast Pacific can be examined from the difference fields between experiments CTL and NoCLD. Note that the first 3-day integration in July is used to spin up the model physics and excluded from our analysis below.

3. Local effects of boundary layer clouds

a. Control simulation

In this subsection we briefly discuss the boundary layer clouds simulated in the control experiment CTL. The large-scale mean surface condition over the southeast Pacific during ASO 1999 is dominated by the subtropical anticyclone centered at about 28°S, 100°W, which drives large-scale southeasterly winds over the southeast Pacific (Fig. 1b). The southeasterlies accelerate on their way toward the equator, giving rise to large-scale divergence and subsidence off the west coast of South America. This large-scale circulation favors the formation and maintenance of both temperature inversion layer and boundary layer clouds in the region (Garreaud et al. 2001). To the north of the equator there is an east–west elongated cyclonic shear zone, where the mean ITCZ is located.

Compared to the Tropical Rain Measuring Mission (TRMM) satellite measurements (Fig. 2a, contours), the model simulated the seasonal mean precipitation quite well both in spatial distribution and magnitude in most of the model domain (Fig. 2b, contours). The model also simulated reasonably well the seasonal

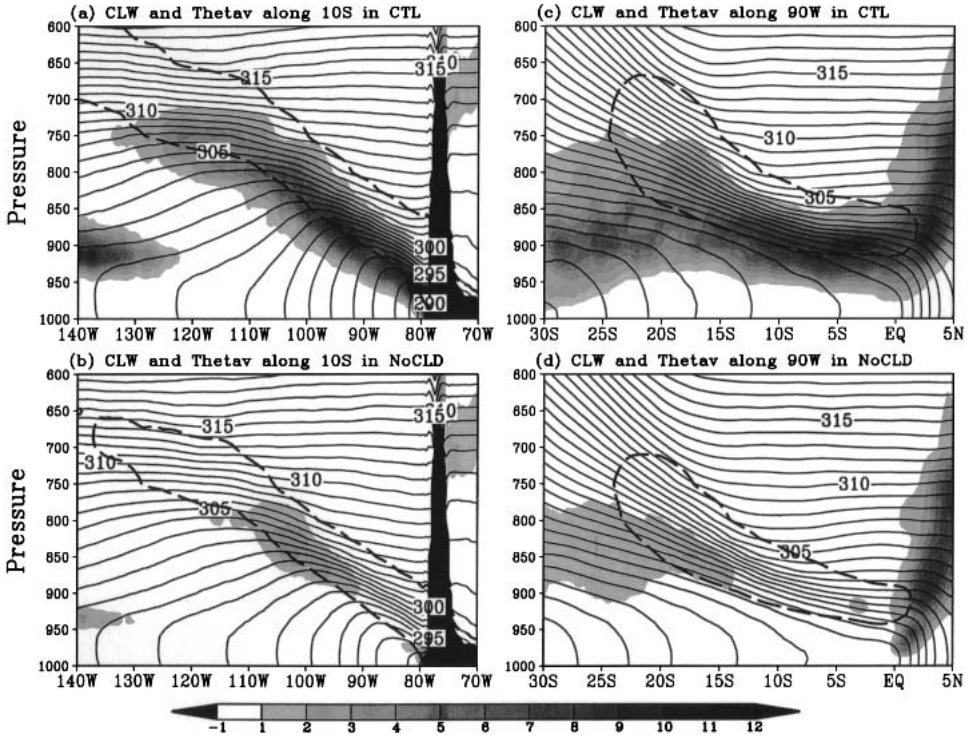

FIG. 3. Vertical cross sections of the ASO averaged cloud water mixing ratio (shaded, unit: 10–2 g kg^{-1}), virtual potential temperature (solid contours in K), along with the $d\theta_v/dp = 8$ K (100 hPa)$^{-1}$ (dashed contours) that is a weaker criterion for temperature inversion, showing zonal cross section along 10°S in (a) CTL and (b) NoCLD, and meridional cross section along 90°W in (c) CTL and (d) NoCLD. The negative value in black shows the model terrain elevation outline (same in Figs. 4–6).

mean column-integrated cloud liquid water content (Fig. 2b, shaded) compared to the TRMM Microwave Imager (TMI) measurements (Fig. 2a, shaded). In particular, the model simulated clouds with little precipitation over large subtropical regions of the southeast Pacific and northeast Pacific, and high cloud water contents with significant precipitation in both the ITCZ region north of the equator and to the southwest corner in the domain where the Southern Hemisphere storm track is located. The model, however, slightly underestimated the cloud water content in the subtropical coastal region off South America and the coastal region just north of the equator, while overestimated the cloud water content in the equatorial region west of the Galapagos Islands.

Despite of some discrepancies, the model reproduced many aspects of the boundary layer clouds over the southeast Pacific. Figure 2c (shaded) shows the simulated cloudiness of low-level clouds below 700 hPa. The model simulated well the boundary layer stratus/SCu with high cloudiness in the coastal regions in the eastern Pacific both off South America and off California coast. The seasonal mean total cloud albedo (Fig. 2c, contours) is relatively high (over 25%–30%) in the stratus/SCu cloud regions and in the ITCZ region north of the equator, consistent with the observed climatological distribution (e.g., Norris 1998).

Figures 3a and 3c show the zonal (along 10°S) and meridional (along 90°W) vertical cross sections of cloud liquid water mixing ratio (shaded) and virtual potential temperature (contours), respectively, together with the $d\theta_v/dp = 8$ K (100 hPa)$^{-1}$ contour (thick dashed curves), which is a weak criterion for the temperature inversion layer. In the zonal direction (Fig. 3a), the well-mixed MBL (vertically constant θ_v) is very shallow with strong temperature inversion off the west coast of South America. The boundary layer cloud deck is topped by the temperature inversion, both increasing in height toward the west (Fig. 3) as SST increases (Fig. 1a), consistent with Paluch et al.'s (1999) dropsonde observations. Note that there apparently were some clouds penetrating into the upper part of the inversion layer. This was due to the fact that all variables shown in Fig. 3 are seasonally averaged in the pressure coordinate.

As already discussed in Wang et al. (2004a,b), there seem different cloud regimes to the east and to the west of 100°W. To the east, the well-mixed MBL is topped by a thick cloud deck, which is capped by a strong temperature inversion layer and accompanied by large low-level cloud amount (Fig. 2d) and high surface drizzle rate (not shown; see Fig. 3d in Wang et al. 2004a). This is typical of marine SCu clouds and is consistent with the underlying cold SST (Albrecht et al. 1995; Stevens et al. 1998; Bretherton et al. 2004). To the

west with warmer SSTs, there is a stable layer between the mixed layer and a weak temperature inversion layer above, trade cumuli embedded in SCu clouds, penetrating through the intermediate stable layer and spreading water vapor and cloud water in the lower part of the inversion layer, indicating a transition from the stratocumulus to trade cumulus regime (Wyant et al. 1997; Stevens et al. 1998). Farther to the west (west of 120°W), two layers of clouds are simulated with the upper one under the inversion layer and the lower one just above the top of the mixed MBL, indicative of a decoupled MBL structure (Krueger et al. 1995; Miller and Albrecht 1995; Wyant et al. 1997; Bretherton and Wyant 1997).

In the meridional direction (Fig. 3c), the temperature inversion height shows a general northward decreasing trend from 20°S to the equator. This decreasing trend of the inversion height seems not due to the weak northward increase in SST up to 5°S (Fig. 1a), but is probably due to the distribution of subtropical subsidence that prevents the inversion height from following the underlying SST. The local maximum in cloud water content corresponds to the local SST maximum around 5°S (Fig. 1a). The equator appears as a local minimum in cloud water content, consistent with observations (Paluch et al. 1999). Note that north of the equator where a strong SST front exists (Fig. 1a), the cloud top rises rapidly as air moves northward toward warmer SSTs (Fig. 3c). South of about 20°S, although the inversion layer rises southward, the cloud base and top change little while with significant decrease in cloud water content. This low-level cloud layer may result from the low lifting condensational level associated with the cold SST over the far southern ocean (Fig. 1a) and the stable stratification above the mixed layer (Fig. 3c), consistent with the observations by Garreaud et al. (2001).

b. *Modification of boundary layer structure by clouds*

With the effect of liquid cloud water on the radiation budget over the eastern Pacific south of the equator removed in the experiment NoCLD, boundary layer clouds over the southeast Pacific are markedly reduced in amount, and they almost disappear east of 100°W (Fig. 2d), indicating the importance of cloud-radiation feedback for boundary layer clouds (Moeng and Lenschow 1995). Although NoCLD fails to simulate the boundary layer cloud deck, it still produces a temperature inversion layer (Figs. 3b,d), implying that processes other than the local cloud-radiation feedback are at work to maintain the temperature inversion in NoCLD. Note that the inversion layer is lower in height and thinner in depth in NoCLD than in CTL. Removal of boundary layer clouds over the southeast Pacific reduces precipitation in the ITCZ region north of the equator, with little effect on either clouds or precipitation over American continents, the Atlantic Ocean and Caribbean Sea (Figs. 2b,d). This interhemispheric interaction between marine boundary layer clouds south of the equator and the ITCZ to the north will be discussed in detail in section 4.

In CTL, boundary layer clouds induce a strong net radiative cooling within and above the cloud layer with a maximum cooling near the temperature inversion base (Figs. 4a,c). By design, the cloud–radiative effect in NoCLD is removed over the southeast Pacific, and the net radiative cooling is small with little vertical variation through the troposphere south of the equator. Figures 5a and 5c show the CTL − NoCLD difference in the net radiative cooling. Boundary layer clouds not only change the radiation budget but also the vertical turbulent mixing, shallow convection, and condensation, and thus modifying the vertical profile of net diabatic heating in the atmosphere. As shown in Figs. 5b and 5d, the net diabatic atmospheric heating/cooling due to the presence of boundary layer clouds is much smaller than the net cloud-induced radiative heating/cooling alone (Figs. 5a,c). The presence of boundary layer clouds gives rise to a net cooling within the inversion layer (Figs. 5b,d). The local response to this net diabatic forcing is a colder MBL and a stronger and higher temperature inversion in CTL than in NoCLD (Figs. 6a,c and 3b,d). The lower troposphere in CTL, compared to NoCLD, moistens within and above the cloud layer but dries slightly in the subcloud layer (Figs. 6b,d), because of cloud-top evaporation, and the enhanced vertical mixing of moisture from the surface layer to the cloud layer and downward mixing of above-inversion dir air (Figs. 6a,c), respectively.

To better understand the modification of boundary layer structure by clouds, we conducted a residual-free heat budget by outputting each term in the following thermodynamic equation from model integration

$$\frac{\partial T}{\partial t} = -\mathbf{V}\cdot\nabla T - \dot{\sigma}\frac{\partial T}{\partial \sigma} + \frac{RT\omega}{pC_{\mathrm{pm}}} + Q_{\mathrm{SW}} + Q_{\mathrm{LW}} + Q_{\mathrm{cond}} + Q_{\mathrm{conv}} + F_T + D_T, \quad (2)$$

where T is the temperature, $\mathbf{V}$ the horizontal wind vector, ∇ the horizontal gradient operator, R the gas constant for dry air, p the pressure, ω the vertical p-velocity, and C_{pm} the specific heat at constant pressure for moist air. The diabatic terms on the right-hand side in the thermodynamic Eq. (2) include shortwave (Q_{SW}) and longwave radiations (Q_{LW}), shallow convection (Q_{conv}), condensation/evaporation (Q_{cond}), vertical turbulent mixing (F_T), and horizontal diffusion of temperature (D_T). Since the horizontal diffusion term is very small compared to other terms, we simply group the first three and the last terms into one as the dynamical warming term (DW), which is the sum of the horizontal and vertical temperature advection, adiabatic warming, and the horizontal diffusion.

Temperature, humidity, and cloud water display large vertical variations following the inversion layer

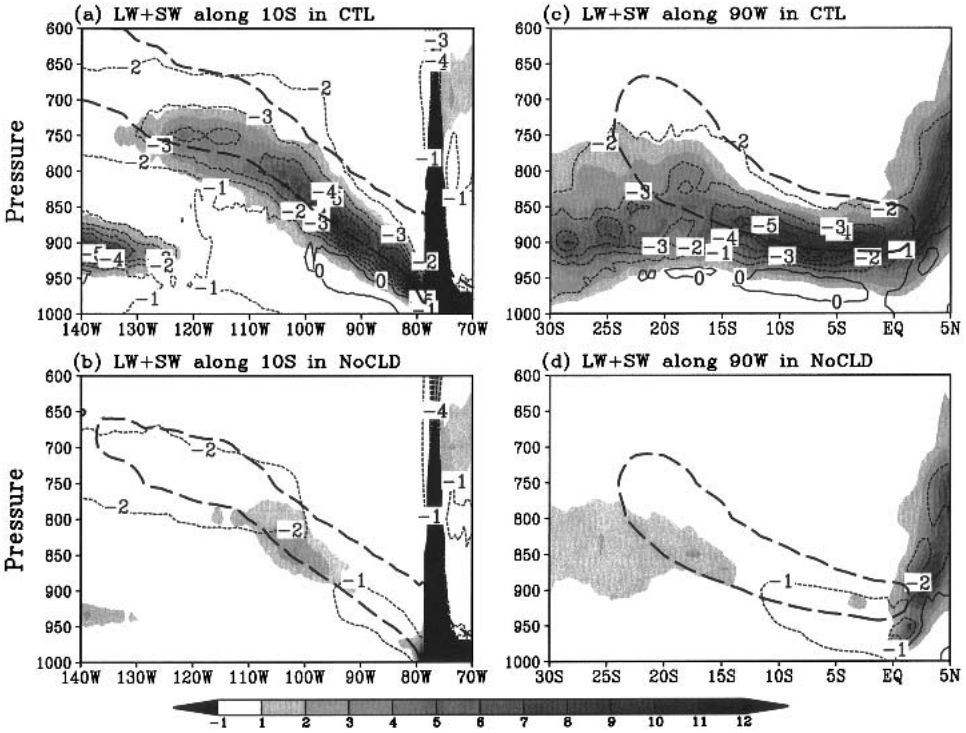

FIG. 4. Zonal and meridional cross sections of shortwave and longwave radiative heating rate (thin contours with contour intervals of 1 K day^{-1}) (a),(b) along 10°S and (c),(d) 90°W, respectively; in (a),(c) CTL and (b),(d) NoCLD. Also shown are cloud water mixing ratio (10^{-2} g kg^{-1}) in shade and the contours for the $d\theta_v/dp = 8$ K (100 hPa)$^{-1}$.

whose height varies strongly both in space and time. Simple averaging in the p coordinate may distort the vertical structure of the planetary boundary layer. Here we make time–space averaging first in a vertical pressure coordinate normalized by the local and instantaneous height (in pressure coordinate) of the inversion base (p_I), $p^* = p/p_I$. Then we project the averaged fields back to the physical space p by using the space–time-averaged value of p_I. This method of averaging preserves the sharp gradients across the inversion. Figure 7 shows some key parameters and the heat budget for CTL (solid) and NoCLD (dashed) averaged using this normalized vertical coordinate for August–October 1999 in a 2° by 2° box (10°–12°S, 90°–92°W) within the central region of the southeast Pacific SCu deck in CTL. The temperature inversion in CTL is much stronger and slightly higher with the cloud water mixing ratio an order of magnitude larger than that in NoCLD (Figs. 7a,b). The vertical structure of cloudiness is consistent with that of the cloud water mixing ratio, with negligible cloudiness in NoCLD (Figs. 7b,c). The air is moister in the cloud layer but slightly drier in the subcloud layer with a deeper well-mixed boundary layer in CTL than in NoCLD (Fig. 7d). The subsidence in the lower troposphere in CTL is larger than that in NoCLD (not shown), indicating an enhancement of subsidence and dynamical warming in response to the net diabatic cooling in CTL.

Although both experiments simulate the temperature inversion layer, the heat balance is quite different. In CTL, the temperature inversion is closely related to the net radiative cooling, which has a maximum cooling rate of more than 10 K day^{-1} at the inversion base (Fig. 7h), while the inversion cap is maintained by the dynamical warming associated with the subsidence which is enhanced by the longwave radiative cooling (Fig. 7i). In NoCLD the net radiative cooling is small (around 2 K day^{-1}) and quite uniform in the vertical, and is not the major mechanism maintaining the temperature inversion. Vertical mixing shows a similar vertical profile, which cools the inversion base except for a deeper mixed layer in CTL than in NoCLD (Fig. 7g). The parameterized shallow convection warms the lower part of the inversion layer but cools the upper part, acting to weaken the inversion, an effect that is stronger in CTL than in NoCLD (Fig. 7f).

The most important difference between CTL and NoCLD is condensational heating (Fig. 7e). In CTL, condensational heating occurs in the cloud layer, with a weak cooling above due to cloud-top evaporation and a strong cooling below due to evaporation of drizzle in the subcloud layer. In NoCLD, however, no condensation occurs in the inversion layer. Instead, there is a strong evaporative cooling centered at the inversion base (Figs. 7g,h), which is associated with the detrainment of cloud water from the top of shallow cumuli,

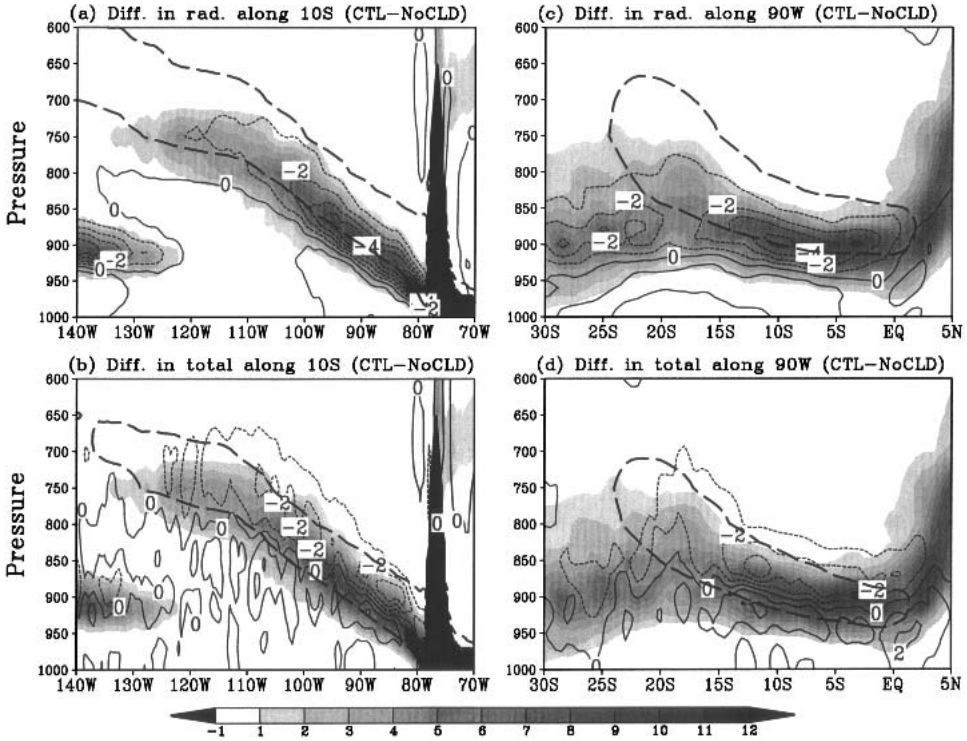

FIG. 5. Zonal and meridional cross sections showing the differences in (a),(c) net radiative heating rate and the (b),(d) total diabatic heating rate between CTL and NoCLD (CTL − NoCLD) (thin contours with contour intervals of 0.5 K day^{-1}) along (a),(b) 10°S and (c),(d) 90°W, respectively. Also shown are cloud water mixing ratio (10^{-2} g kg^{-1}) in shade and the contours for the $d\theta_v/dp = 8$ K (100 hPa)$^{-1}$ in CTL.

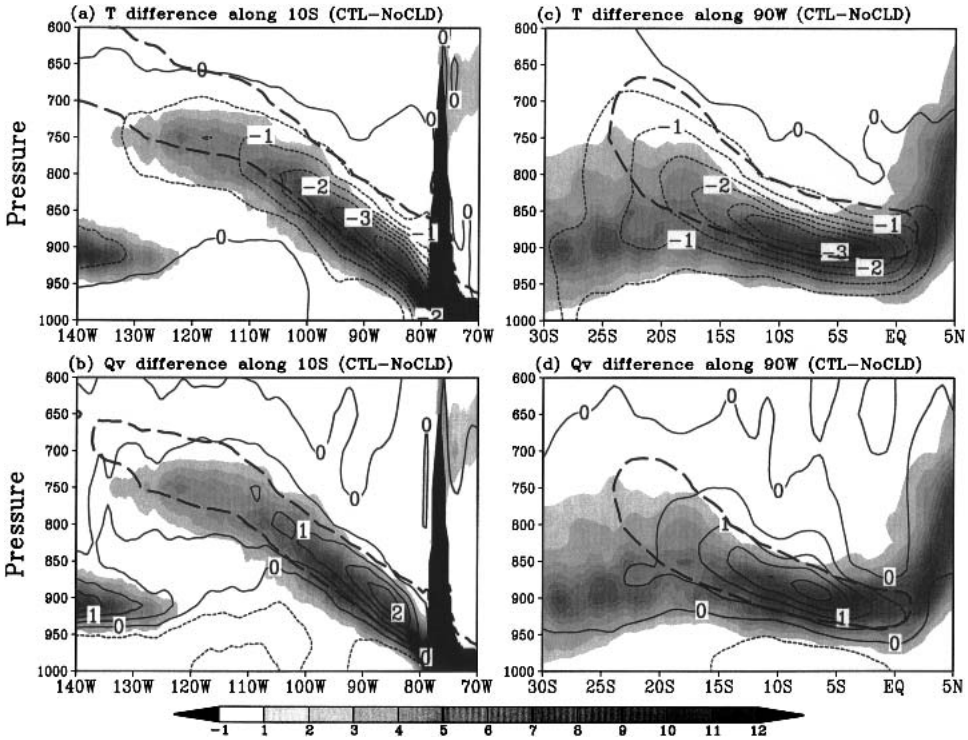

FIG. 6. As in Fig. 5, but for the differences in (a),(c) air temperature and (b),(d) water vapor mixing ratio.

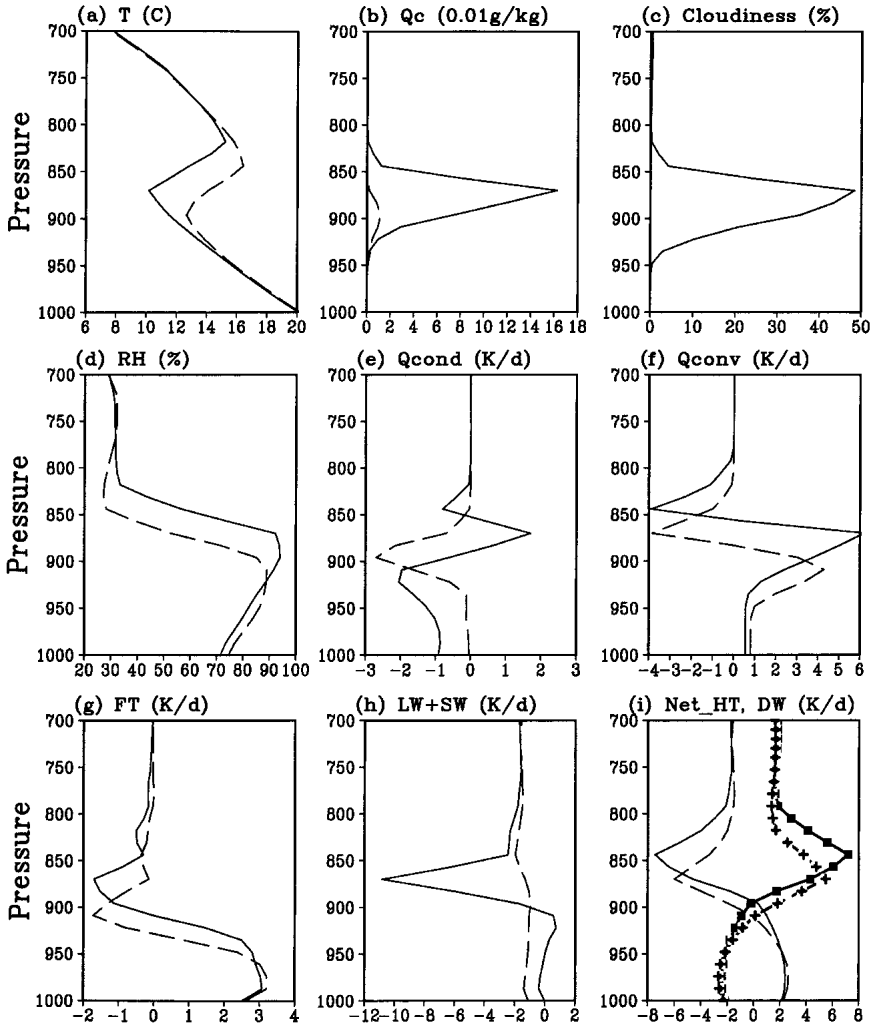

FIG. 7. Some key parameters and the heat budget with normalized vertical coordinate and averaged in a 2° by 2° box (10°–12°S, 90°–92°W) in ASO for CTL (solid curves) and NoCLD (dashed curves): (a) air temperature (K), (b) cloud water mixing ratio (10^{-2} g kg^{-1}), (c) cloudiness (percentages), (d) relative humidity (percentages), and heating rate (K day^{-1}) due to (e) condensation/evaporation, (f) shallow convection, (g) vertical turbulent mixing, (h) longwave and shortwave radiation, and (i) the net diabatic heating rate (K day^{-1}) and the corresponding dynamical warming (K day^{-1}) with diamonds for CTL and crosses for NoCLD.

which occasionally penetrate into the temperature inversion layer. This evaporation due to the detrainment of the shallow cumulus top plays an important role in maintaining the inversion in NoCLD (Figs. 7a,e,f).

In both CTL and NoCLD, the dynamical warming associated with the large-scale subsidence is important for the inversion formation (Fig. 7i). The net heating profile is similar in CTL and NoCLD with a net cooling in the inversion layer and a net warming in the mixed layer (Fig. 7i), but the cooling is deeper and stronger in CTL, indicating that a stronger descending motion and the associated dynamical warming are required to balance this cooling and a stronger vertical mixing that prevents a too low inversion/cloud layer (Fig. 7i).

In summary, the cloud radiative effect is the key to maintaining both the strong temperature inversion and boundary layer clouds in CTL. The net diabatic cooling (Fig. 7i) by boundary layer clouds is, however, much smaller than the net radiative cooling because of the drizzle-induced condensational heating in the cloud layer (Fig. 7e) and convective turbulent entrainment penetrating into the temperature inversion layer (Fig. 7f). In our control simulation, the evaporation of drizzle plays a role in destabilizing the subcloud layer, increasing the surface sensible heat flux. These further promote the development of shallow convection, which penetrates into the inversion layer to enhance cloud-top entrainment. The latter may be further enhanced by the destabilizing effect due to cloud-top radiative and evaporative cooling. Therefore, both drizzle and

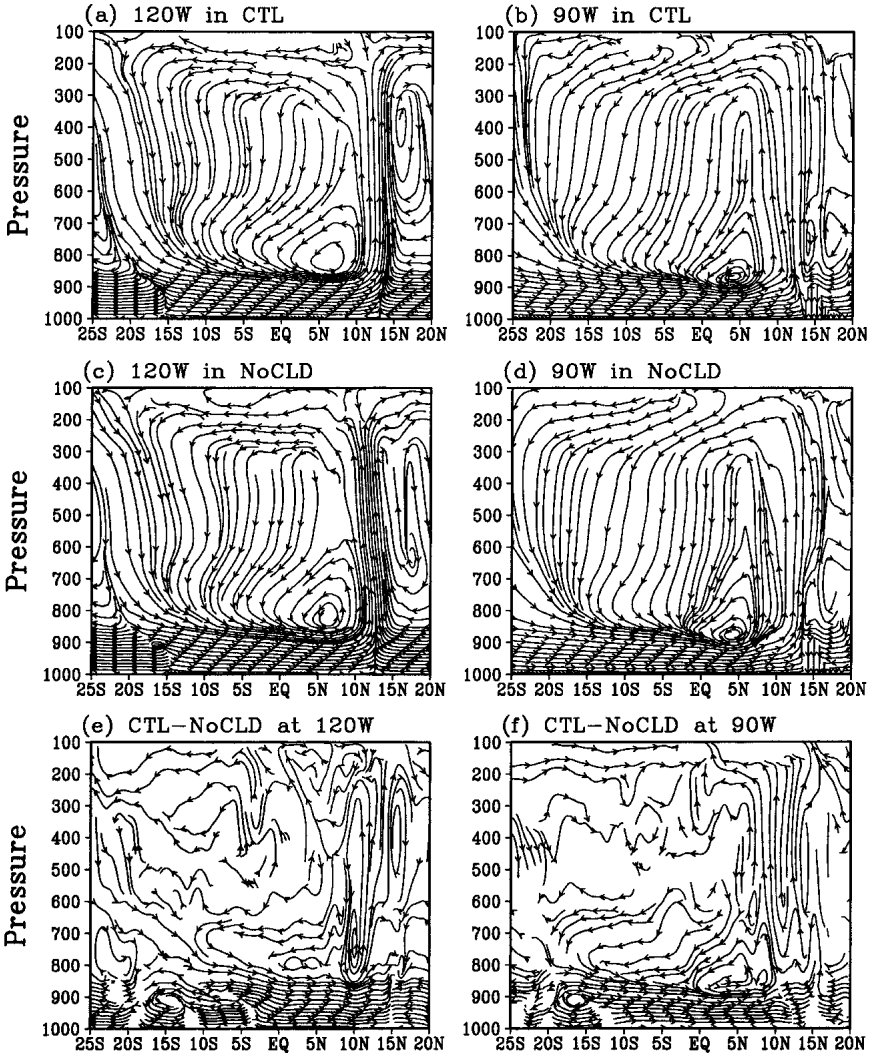

FIG. 8. Streamlines in the meridional vertical plane along 120° and 90°W, showing the large-scale meridional circulation in experiments (a),(b) CTL and (c),(d) NoCLD. (e), (f) The differences between the CTL and NoCLD experiments at 120° and 90°W.

cloud-top entrainment are important in our heat budget in the simulated boundary layer clouds. The importance of parameterized shallow convection to the realistic simulation of subtropical marine SCu has also been emphasized by McCaa and Bretherton (2004) and Wang et al. (2004b).

4. Large-scale atmospheric forcing by boundary layer clouds

This section examines the large-scale atmospheric forcing induced by boundary layer clouds over the southeast Pacific by comparing CTL with NoCLD. Both experiments simulate the local meridional Hadley circulation over the eastern Pacific, with lower tropospheric southerly flow from Southern Hemisphere, converging onto the ITCZ between 10° and 15°N. The air rises in the ITCZ, then turns southward to the Southern Hemisphere in the upper troposphere, and finally descends in the subtropical region between 10° and 25°S (Fig. 8). In addition to the large-scale deep Hadley circulation, both experiments produce a shallow meridional circulation in the lower troposphere (Figs. 8a–c). The shallow circulation has a zonal variation in the meridional extent. Over the strong SST front east of about 105°W (Fig. 1a), it is mainly confined between the northern ITCZ and 5°S (Figs. 8b,d). To the west, however, it penetrates into 15°S (Figs. 8a,c). The shallow circulation also has a tendency to increase its height toward the west (Figs. 8a,b, or Figs. 8c,d). This trend seems to be correlated with the increases in SST and the inversion height toward the west (Figs. 1a, and 3a,b).

A similar shallow meridional circulation in the same

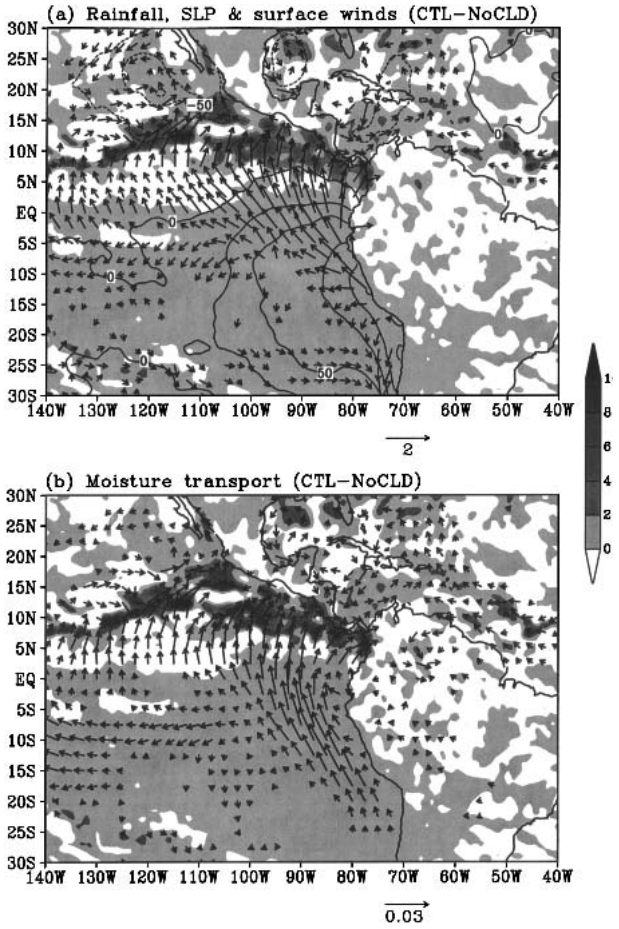

FIG. 9. (a) Differences in ASO mean daily rainfall (shaded in mm day^{-1}), sea level pressure (contours in Pa), and the 10-m-height winds (vectors with unit vector of 2 m s^{-1}) between CTL and NoCLD (CTL−NoCLD); (b) difference in column-integrated moisture transport (vectors with unit vector of 0.03 kg kg^{-1} m s^{-1}) between CTL and NoCLD superposed onto difference in rainfall as in (a).

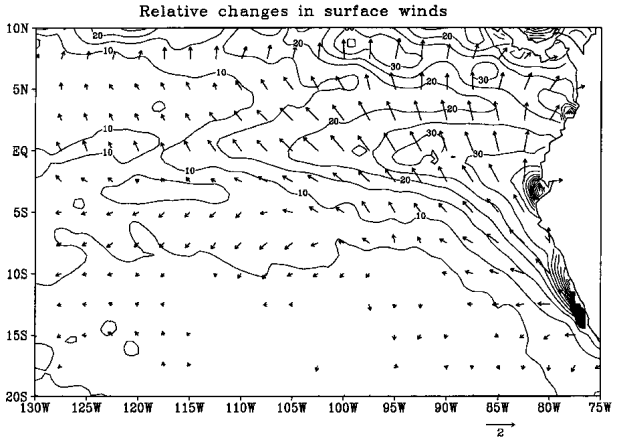

FIG. 10. Relative changes (in percentages) in 10-m-height wind speed between CTL and NoCLD (contours) and differences in 10-m-height winds (vectors, unit vector: 2 m s^{-1}) between CTL and NoCLD (CTL − NoCLD) as shown in Fig. 9a. For clarity, only the tropical equatorial region is shown.

region was previously identified by Murakami et al. (1992), who attributed it to the local adjustment of pressure to the large SST gradients across the equator. Tomas and Webster (1997) attribute a similar shallow meridional circulation in divergent wind to the advection of absolute vorticity. Trenberth et al. (2000) found the shallow meridional circulations in many tropical regions from global reanalyzes. More recently, Zhang et al. (2004) documented the shallow circulation cell in the eastern Pacific based on four independent datasets and found that both the strength and depth of this circulation cell undergo a distinct annual cycle. As noted by Zhang et al. that the dynamics of the shallow meridional circulation at large remains unknown although it may have significant climatic implications in the tropical eastern Pacific. A full investigation of the mechanism for the formation of the shallow meridional circulation is beyond the scope of this study and will be one of our future foci. Here, we will examine how the presence of boundary layer clouds south of the equator enhances the shallow meridional circulation as seen in Figs. 8e and 8f.

As discussed in section 3, the net cloud-induced cooling and the enhanced cold advection in the subcloud layer cool the lower troposphere over the southeast Pacific (Figs. 6a,c). As a result of hydrostatic adjustment, a local anomalous high pressure system in the boundary layer develops centered at about 15°S, 90°W (Fig. 9a). The equatorward pressure gradient associated with this anomalous boundary layer high pressure system drives the anomalous boundary layer southeasterly flow in the tropical eastern Pacific (Fig. 9a), enhancing the background southeast trade winds (Fig. 1b). The enhanced boundary layer winds increase moisture convergence in the northern ITCZ region (Fig. 9b), enhancing convection and precipitation in the ITCZ, which is slightly shifted northward due to the stronger cross-equatorial flow in CTL than in NoCLD (shaded in Fig. 9) between 95° and 125°W. The light precipitation anomalies over the southeast Pacific are due to drizzle under the boundary layer cloud deck in CTL (Wang et al. 2004a). The anomalous low pressure system centered at about 20°N, 115°W north of the ITCZ (Fig. 9a) is due to the Rossby wave response to the enhanced convective heating in the ITCZ (e.g., Gill 1980).

Figure 10 shows the relative changes in surface wind speed. In a large area over the equatorial eastern Pacific, wind speeds are increased by 10%–20% due to the presence of southeast Pacific boundary layer clouds. Even larger increases occur in the coastal region south of the equator and in the cold-tongue region. Since both coastal and equatorial upwelling are very sensitive to the southerly winds, our results imply that boundary layer clouds could induce even larger changes in a

coupled ocean–atmosphere model than what we show here.

Sensible and latent heat fluxes at the ocean surface are also modified due to the presence of southeast Pacific boundary layer clouds as a result of changes in surface winds and turbulent fluxes in the subcloud layer as discussed in section 3. The surface latent heat flux is increased both in the ITCZ region and over the southeastern Pacific with the maximum increase near the eastern Pacific equatorial SST front (Figs. 1a and 11a), consistent with the enhanced surface winds in the region (Fig. 9a). This increased latent heat flux appears to be responsible for the increased precipitation in the ITCZ to the north off the west coast (Fig. 9a). The sensible heat flux is slightly increased in the coastal region off South America and over the subtropical southeastern Pacific (Fig. 11b).

As seen from Figs. 8e and 8f, the presence of boundary layer clouds produces an anomalous meridional circulation in the lower troposphere, which enhances the already existing shallow meridional circulation cell (Figs. 8a,b). Although its depth slightly increases toward the west due to the westward slope of the net cloud-induced cooling (Fig. 5b), the anomalous meridional circulation has the return flow originates from the ITCZ north of the equator and is the strongest at about 700 hPa (Figs. 8e,f). A horizontal view of the anomalous winds and geopotential height at both 1000 and 700 hPa is shown in Fig. 12. Note that both the anomalous winds and geopotential height at 1000 hPa (Fig. 12a) are similar to the anomalous surface winds and pressure shown in Fig. 9a. At 700 hPa (Fig. 12b), a negative geopotential height anomaly is located in the subtropical region in the southeast Pacific between 10°–30°S, indicating a baroclinic structure of the anomalous shallow circulation. The cross-equatorial northerly return flow is strong to the west of 90°W and is dominated by northwesterlies to the west of about 105°W, indicating that the anomalous meridional circulation is not a complete circulation cell. Therefore, only the zonal mean has the physical meaning of the meridional mass circulation. As such in the following discussion, we define the anomalous meridional circulation as that of the zonal mean between 85° and 125°W.

Figure 13 shows the seasonal mean rainfall averaged between 85° and 125°W from CTL (thick solid) and NoCLD (solid dashed), together with the difference (CTL minus NoCLD) in the column-integrated moisture convergence between CTL and NoCLD. As already seen from Fig. 9, with radiatively active boundary layer clouds over the eastern Pacific south of the equator, rainfall in the ITCZ region north of the equator is increased by 15%–20% between 7° and 12°N. The increased rainfall in CTL is consistent with the increase (CTL − NoCLD) in the column-integrated moisture convergence (thin dashed curve in Fig. 13) due to the enhanced cross-equatorial flow in the moisture-laden surface layer (Fig. 9).

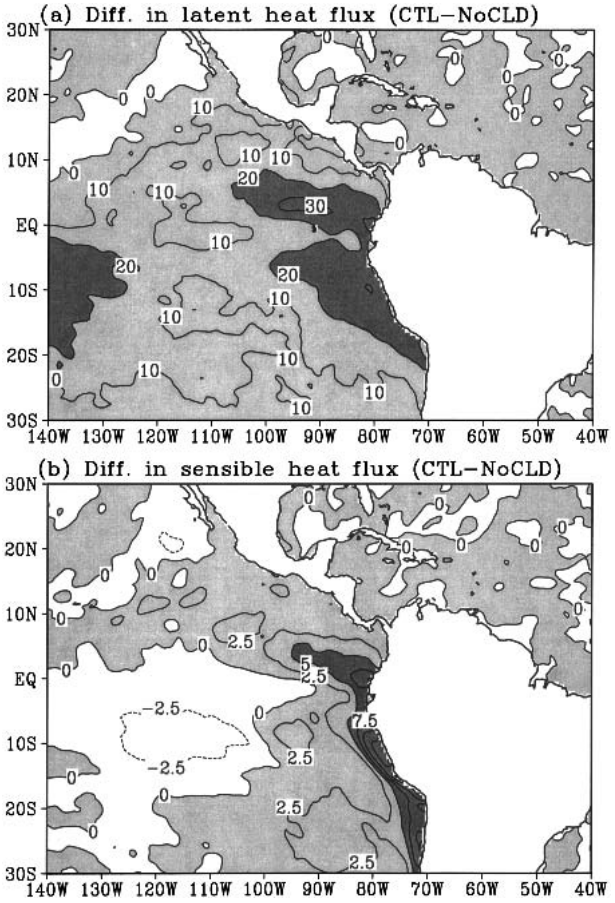

FIG. 11. Differences between the CTL and NoCLD (CTL−NoCLD) in (a) surface latent and (b) sensible heat fluxes (W m^{-2}), with positive regions shaded.

Figure 14 shows the vertical meridional cross section of differences in net diabatic heating rate (contours) between CTL and NoCLD (CTL − NoCLD) and the corresponding anomalous vertical meridional circulation (arrows) averaged between 85° and 125°W as in Fig. 13. South of the equator, the net cloud-induced cooling results in an anomalous descending motion just above the cloud layer south of the equator. An anomalous shallow meridional circulation below 600 hPa thus develops in response to the cross-equatorial differential heating induced by boundary layer clouds south of the equator. The weak descending motion in the cloud layer south of the equator produces dynamical warming to balance the net cloud-induced diabatic cooling. The boundary layer southerly, as the lower branch of the shallow meridional circulation, accelerates equatorward and converges onto the updrafts in the ITCZ around 10°N. A returning flow at the top of the cooling layer blows southward from the ITCZ region and joins the subsidence in the cloud layer south of the equator. This shallow meridional circulation enhances the local lower tropospheric meridional circulation shown in Fig. 8.

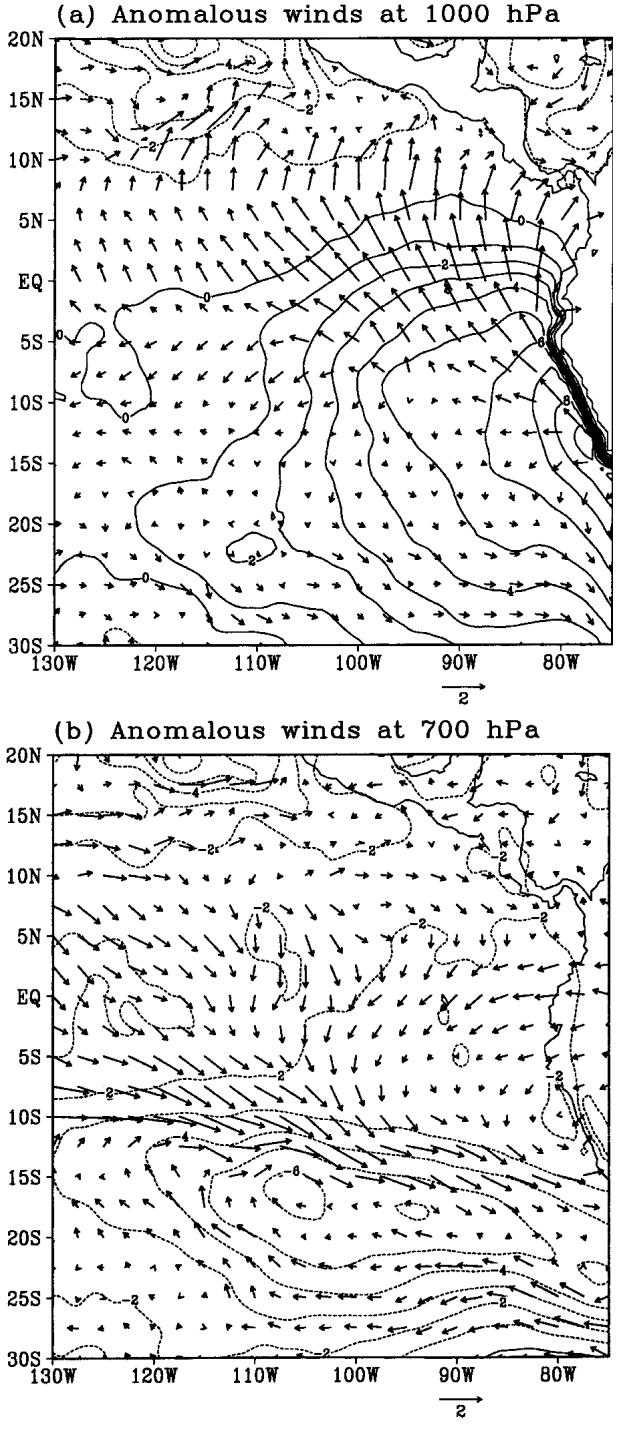

FIG. 12. Differences in ASO mean winds (vectors with unit vector of 2 m s^{-1}) between CTL and NoCLD (CTL−NoCLD) at (a) 1000 and (b) 700 hPa.

In addition to the shallow anomalous meridional circulation, consistent with the rainfall increase in the ITCZ region, a deep anomalous heating appears around 12°N with a deep anomalous upward motion (Fig. 14), which seems to enhance the local deep Hadley circulation (Fig. 8). The air in the ITCZ updrafts turns equatorward and transports mass to the Southern Hemisphere in the upper troposphere where air descends very slowly in the subtropical region. This enhancement of the local Hadley circulation may play some role in enhancing and maintaining boundary layer clouds south of the equator, as hypothesized by Nigam (1997). Note also that the net diabatic heating in the subcloud layer is balanced by the increased cold advection due to the enhanced boundary layer southerly flow, while a local anomalous heating maximum in the boundary layer between the equator and 5°N in Fig. 14

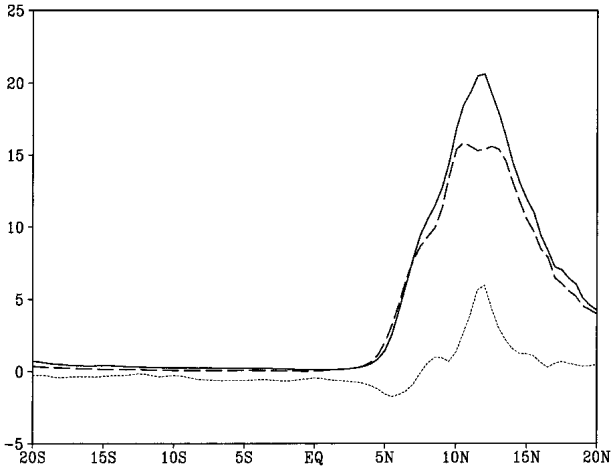

FIG. 13. Meridional distributions of ASO mean daily rainfall (mm day^{-1}) in CTL (solid) and NoCLD (dashed) and the difference in column-integrated moisture convergence (10^{-2} g m^{-1} s^{-1}) between CTL and NoCLD (dotted) averaged between 85° and 125°W.

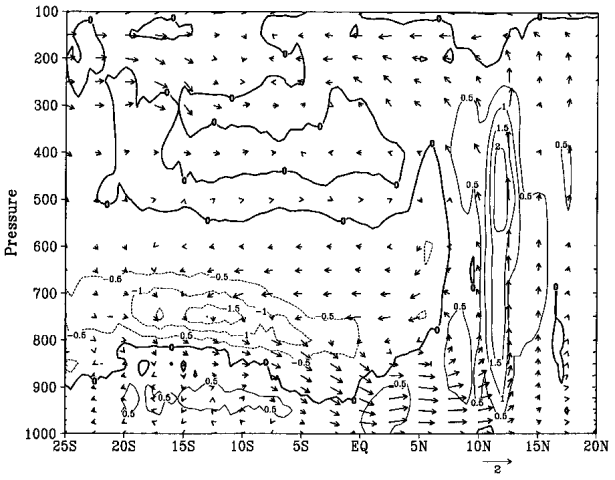

FIG. 14. Meridional vertical cross section of the net cloud-induced diabatic heating rate (contours in K day^{-1} with negative values dashed) and the meridional circulation averaged between 85° and 125°W. The unit vector represents 2 m s^{-1} for meridional wind and 8 mm s^{-1} for vertical wind.

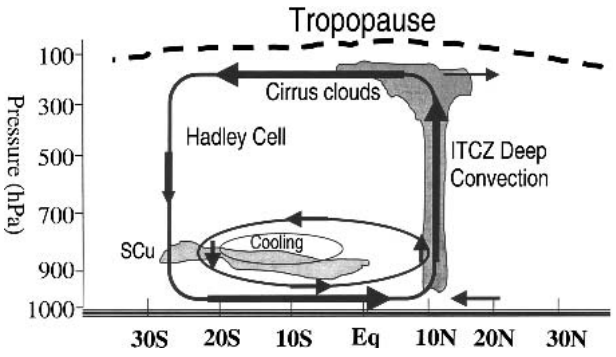

FIG. 15. A schematic diagram showing the large-scale atmospheric forcing of the MBL clouds over the southeast Pacific off South America in shaping the eastern Pacific climate. The reference pressure is shown to the left. The thick dashed line at the top shows the tropopause. The thick arrows show the circulation in the Hadley cell. The shaded area south of the equator at about 900 hPa shows the SCu clouds. Deep shaded cloud feature around 10°N indicates the deep convection in the ITCZ with the cirrus clouds at the top in the outflow region below tropopause. The small oval at the upper part of the SCu clouds indicates net cooling due to the presence of the SCu clouds. The circulation in the lower troposphere below 700 hPa shows the anomalous meridional shallow circulation driven by the cloud-top cooling. See the text for details.

is caused by the increased surface sensible heat flux as seen from Fig. 11b.

5. Summary and discussion

a. Summary

The IPRC–RegCM is used to study the effect of the southeast Pacific boundary layer cloud deck on both the local boundary layer structure and the large-scale atmospheric circulation during August–October 1999. We have investigated both the local and remote responses to net cloud-induced diabatic cooling (including longwave radiation, condensational heating, vertical turbulent mixing, and boundary layer cumulus effects). The control run simulates reasonably well the large-scale circulation over the eastern Pacific, precipitation in the ITCZ north of the equator, and extensive marine boundary layer clouds and temperature inversion over the southeast Pacific. The strength of the inversion capping is not only determined by large-scale subsidence and local SSTs, but by the cloud–radiation feedback as well. With the cloud–radiative effect over the southeast Pacific artificially removed, boundary layer clouds almost disappear south of the equator and precipitation in the ITCZ north of the equator is reduced by 15%–20% over the eastern Pacific.

The large-scale atmospheric forcing induced by southeast Pacific boundary layer clouds and its effect on the eastern Pacific climate can be summarized schematically in Fig. 15. Boundary layer clouds south of the equator induce an in situ net diabatic cooling effect in the lower troposphere between 900 and 700 hPa. A high boundary layer pressure anomaly develops under the clouds in response to the atmospheric cooling above and its associated equatorward gradient enhances cross-equatorial southeasterly flow in the boundary layer over the tropical eastern Pacific. This enhanced southeasterly flow increases the moisture convergence, and hence convection in the ITCZ north of the equator, with a southward returning flow at the top of the boundary layer and a descending motion over the southeast Pacific. The deep local Hadley circulation strengthens in response to the enhanced deep convection in the ITCZ. The enhanced subsidence due to both the anomalous shallow meridional circulation and the deep Hadley circulation can in turn help maintain the temperature inversion and the boundary layer clouds over the southeast Pacific. Thus, a positive feedback forms between the forced large-scale meridional circulation and the boundary layer clouds south of the equator, as hypothesized by Nigam (1997). This positive feedback favors the ITCZ displaced to the Northern Hemisphere (provided that the boundary layer clouds first develop south of the equator), reinforcing the interhemispheric climate asymmetry over the tropical eastern Pacific.

b. Discussion

With a linear steady state primitive equation model, Nigam (1997) reported an enhancement of low-level southerly flow over the equatorial eastern Pacific in response to the March to May cooling in the lower troposphere (600–900 hPa), which was regarded as longwave radiative cooling by low-level SCu clouds over the southeast Pacific. The cooling that Nigam diagnosed was slightly more than 1 K day^{-1} in the eastern equatorial Pacific (see his Fig. 2c). The surface southerly flow forced by this cooling in his linear model was greater than 1 m s^{-1}. In our simulation, the maximum net cloud-induced cooling in the most extensive SCu cloud region is about 2 K day^{-1} (Figs. 5b,d and 7i). It drives an anomalous surface southerly flow of about 2 m s^{-1} (Fig. 9a), quite consistent with Nigam's linear calculations. We note, however, that the net cloud-induced cooling is about one-fifth of the longwave radiative cooling because of the opposing effects of condensational heating in the clouds and convective turbulent entrainment across the inversion layer.

Bergman and Hendon (2000) found in a linear atmospheric model that more than half of the observed strength of meridional circulation in the tropical eastern Pacific is due to radiative forcing by boundary layer clouds. The SCu cloud forcing and the atmospheric response to it are much weaker in our physically based model that includes both radiation and latent heat effects of the SCu clouds. In contrast to the linear calculations by Bergman and Hendon where circulation forced by boundary layer cloud cooling was confined in the lower troposphere, our results show that the cloud

forcing has a deep effect throughout the troposphere, as the strengthened cross-equatorial surface flow enhances ITCZ convection.

The interaction between southeast Pacific SCu clouds and the ITCZ can enhance the interhemispheric climate asymmetry over the tropical eastern Pacific, where the ITCZ is permanently displaced in the Northern Hemisphere. It is generally believed that the continental forcing of South and North Americas triggers the latitudinal climate asymmetry (e.g., Philander et al. 1996; Wang and Wang 1999; Xie and Saito 2001). Then air–sea coupled processes act to amplify this climatic asymmetry, such as the wind–evaporation–SST feedback (Xie and Philander 1994), the coastal upwelling–wind feedback, and the boundary layer clouds–SST feedback (Philander et al. 1996; Li 1997). The boundary layer cloud—circulation feedback discussed in this study may serve as an additional amplifier for the climatic asymmetry in the eastern Pacific. For instance, the enhanced southeast Pacific SCu clouds can increase surface latent heat flux, lowering local SST in the equatorial cold-tongue region; the enhanced southeasterly coastal winds can enhance the coastal upwelling and cool the SST there; boundary layer clouds can reduce the shortwave radiation reaching the ocean surface and cool the underlying SST. SST cooling south of the equator increases SST gradient, leading to a further enhancement of the southeasterly trades. A full evaluation of the boundary layer cloud effect, however, needs an elaborate coupled ocean–atmosphere model.

Note also that the anomalous shallow meridional circulation due to the presence of boundary layer clouds over the southeast Pacific discussed in this study is different from the shallow meridional circulation cell discussed by Tomas and Webster (1997), Trenberth et al. (2000), and Zhang et al. (2004). The latter showed the actual shallow meridional circulation in the lower troposphere, as seen in our Figs. 8a and 8b, while the anomalous shallow circulation discussed in this study is the one forced by the net cloud-induced cooling. In reality, this forced anomalous shallow meridional circulation may contribute to the total shallow circulation observed in this region. Therefore, the results from this study indicate that the presence of boundary layer clouds over the southeast Pacific off South America can enhance the shallow meridional circulation cell observed by Zhang et al. (2004). The precise formation mechanisms for the shallow circulation cell, however, are still unknown and needs further investigation.

Finally, we should point out that although the model results, especially the simulation of boundary layer clouds, are not perfect and can be sensitive to a number of model parameters and model physical parameterization schemes (Wang et al. 2004a,b), we feel that the overall results, especially the large-scale response to the cloud-top longwave radiative cooling, would not be altered qualitatively by the choice of parameters and schemes. Future studies are required to investigate the detailed boundary layer cloud processes in physically based models that incorporate the improved understanding of cloud-topped boundary layer from previous single column models and large-eddy simulations.

Acknowledgments. The authors are grateful to two anonymous reviewers for their comments, which helped improve the manuscript. This study is supported by NOAA/PACS Program (NA17RJ230), NASA (NAG5-10045 and JPL Contract 1216010), and the Frontier Research System for Global Change through its sponsorship of the International Pacific Research Center (IPRC) in the School of Ocean and Earth Science and Technology (SOEST) at the University of Hawaii.

REFERENCES

Albrecht, B. A., M. P. Jensen, and W. J. Syrett, 1995: Marine boundary layer structure and fractional cloudiness. *J. Geophys. Res.,* **100** (D7), 14 209–14 222.

Bachiochi, D. R., and T. N. Krishnamurti, 2000: Enhanced low-level stratus in the FSU coupled ocean–atmosphere model. *Mon. Wea. Rev.,* **128,** 3083–3103.

Bergman, J. W., and H. H. Hendon, 2000: Cloud radiative forcing of the low-latitude tropospheric circulation: Linear calculations. *J. Atmos. Sci.,* **57,** 2225–2245.

Bretherton, C. S., and M. C. Wyant, 1997: Moisture transport, lower tropospheric stability, and decoupling of cloud-topped boundary layers. *J. Atmos. Sci.,* **54,** 148–167.

——, and Coauthors, 2004: The EPIC 2001 stratocumulus study. *Bull. Amer. Meteor. Soc.,* **85,** 967–977.

Chou, M., M. J. Suarez, C.-H. Ho, M. M.-H. Yan, and K.-T. Lee, 1998: Parameterizations for cloud overlapping and shortwave single-scattering properties for use in general circulation and cloud ensemble models. *J. Climate,* **11,** 202–214.

Dickinson, R. E., A. Henderson-Sellers, and P. J. Kennedy, 1993: Biosphere-atmosphere transfer scheme (BATS) version 1e as coupled to the NCAR Community Climate Model. NCAR Tech. Note NCAR/TN-387+STR, National Center for Atmospheric Research, 72 pp.

Edwards, J. M., and A. Slingo, 1996: Studies with a flexible new radiation code. Part I: Choosing a configuration for a large-scale model. *Quart. J. Roy. Meteor. Soc.,* **122,** 689–719.

Garreaud, R. D., J. Rutllant, J. Quintana, J. Carrasco, and P. Minnis, 2001: CIMAR-5: A snapshot of the lower troposphere over the subtropical southeast Pacific. *Bull. Amer. Meteor. Soc.,* **82,** 2193–2207.

Gill, A. E., 1980: Some simple solutions for heat-induced tropical circulation. *Quart. J. Roy. Meteor. Soc.,* **106,** 447–462.

Giorgi, F., and G. T. Bates, 1989: The climatological skill of a regional model over complex terrain. *Mon. Wea. Rev.,* **117,** 2325–2347.

Gordon, C. T., A. Rosati, and R. Gudgel, 2000: Tropical sensitivity of a coupled model to specified ISCCP low clouds. *J. Climate,* **13,** 2239–2260.

Gregory, D., J.-J. Moncrette, C. Jakob, A. C. M. Beljaars, and T. Stockdale, 2000: Revision of the convection, radiation and cloud schemes in the ECMWF model. *Quart. J. Roy. Meteor. Soc.,* **126,** 2685–1710.

Kalnay, E., and Coauthors, 1996: The NCEP/NCAR 40-Year Reanalysis Project. *Bull. Amer. Meteor. Soc.,* **77,** 437–471.

Kessler, E., 1969: *On the Distribution and Continuity of Water Substance in Atmospheric Circulation. Meteor. Monogr.,* No. 32, Amer. Meteor. Soc., 84 pp.

Klein, S. A., and D. L. Hartmann, 1993: The seasonal cycle of low stratiform clouds. *J. Climate,* **6,** 1587–1606.

Krueger, S. K., G. T. McLean, and Q. Fu, 1995: Numerical simulation of the stratus-to-cumulus transition in the subtropical marine boundary layer. Part I: Boundary-layer structure. *J. Atmos. Sci.,* **52,** 2839–2850.

Langland, R. H., and C.-S. Liou, 1996: Implementation of an E-ε parameterization of vertical subgrid-scale mixing in a regional model. *Mon. Wea. Rev.,* **124,** 905–918.

Li, T., 1997: Air–sea interactions of relevance to the ITCZ: Analysis of coupled instabilities and experiments in the hybrid coupled GCM. *J. Atmos. Sci.,* **54,** 134–147.

Lin, Y.-L., R. D. Farley, and H. D. Orville, 1983: Bulk parameterization of the snow field in a cloud model. *J. Climate Appl. Meteor.,* **22,** 1065–1092.

Ma, C.-C., C. R. Mechoso, A. W. Roberton, and A. Arakawa, 1996: Peruvian stratus clouds and the tropical Pacific circulation—A coupled ocean–atmosphere GCM study. *J. Climate,* **9,** 1635–1645.

McCaa, J. R., and C. S. Bretherton, 2004: A new parameterization for shallow cumulus convection and its application to marine subtropical cloud-topped boundary layer. Part II: Regional simulation of marine boundary layer clouds. *Mon. Wea. Rev.,* **132,** 883–896.

Miller, M. A., and B. A. Albrecht, 1995: Surface-based observations of mesoscale cumulus–stratocumulus interaction during ASTEX. *J. Atmos. Sci.,* **52,** 2809–2826.

Moeng, C.-H., 2000: Entrainment rate, cloud fraction, and liquid water path of PBL stratocumulus clouds. *J. Atmos. Sci.,* **57,** 3627–3643.

——, and D. H. Lenschow, 1995: Numerical investigation of the roles of radiative and evaporative feedbacks in stratocumulus entrainment and breakup. *J. Atmos. Sci.,* **52,** 2869–2883.

Murakami, T., B. Wang, and S. W. Lyons, 1992: Contrasts between summer monsoons over the Bay of Bengal and the eastern North Pacific. *J. Meteor. Soc. Japan,* **70,** 191–210.

Nigam, S., 1997: The annual warm to cold phase transition in the eastern equatorial Pacific: Diagnosis of the role of stratus cloud-top cooling. *J. Climate,* **10,** 2447–2467.

Nordeng, T. E., 1995: Extended versions of the convective parameterization scheme at ECMWF and their impact on the mean and transient activity of the model in the Tropics. ECMWF Research Department Tech. Memo. 2006, 41 pp.

Norris, J. R., 1998: Low cloud structure over the ocean from surface observations. Part II: Geographical and seasonal variations. *J. Climate,* **11,** 383–403.

Paluch, L. R., G. McFarquhar, and D. H. Lenschow, 1999: Marine boundary layers associated with ocean upwelling over the eastern equatorial Pacific Ocean. *J. Geophys. Res.,* **104** (D24), 30 913–30 936.

Philander, S. C. H., D. Gu, D. Halpern, G. Lambert, N.-C. Lau, T. Li, and R. C. Pacanowski, 1996: Why the ITCZ is mostly north of the equator. *J. Climate,* **9,** 2958–2972.

Randall, D. A., J. A. Coakley Jr., C. W. Fairall, R. A. Kropfli, and D. H. Lenschow, 1984: Outlook for research on subtropical marine stratiform clouds. *Bull. Amer. Meteor. Soc.,* **65,** 1290–1301.

Reisner, J., R. M. Rasmussen, and R. T. Bruintjes, 1998: Explicit forecasting of supercooled liquid water in winter storms using the MM5 mesoscale model. *Quart. J. Roy. Meteor. Soc.,* **124,** 1071–1107.

Reynolds, R. W., and T. M. Smith, 1994: Improved global sea surface temperature analyses using optimum interpolation. *J. Climate,* **7,** 929–948.

Rockel, B., E. Raschke, and B. Weyres, 1991: A parameterization of broad band radiative transfer properties of water, ice and mixed clouds. *Beitr. Phys. Atmos.,* **64,** 1–12.

Rutledge, S. A., and P. V. Hobbs, 1983: The mesoscale and microscale structure and organization of clouds and precipitation in midlatitude cyclones. Part VIII: A model for the "seeder-feeder" process in warm-frontal rainbands. *J. Atmos. Sci.,* **40,** 1185–1206.

Slingo, A., and H. M. Schrecker, 1982: On the shortwave radiative properties of water clouds. *Quart. J. Roy. Meteor. Soc.,* **108,** 407–426.

Small, R. J., S.-P. Xie, and Y. Wang, 2003: Numerical simulation of atmospheric response to Pacific tropical instability waves. *J. Climate,* **16,** 3722–3737.

Stevens, B., W. R. Cotton, G. Feingold, and C.-H. Moeng, 1998: Large-eddy simulations of strongly precipitating, shallow, stratocumulus-topped boundary layer. *J. Atmos. Sci.,* **55,** 3616–3638.

——, and Coauthors, 2003: On entrainment rates in nocturnal marine stratocumulus. *Quart. J. Roy. Meteor. Soc.,* **129,** 3469–3485.

Sun, Z., and K. Shine, 1994: Studies of the radiative properties of ice and mixed phase clouds. *Quart. J. Roy. Meteor. Soc.,* **120,** 111–137.

——, and L. Rikus, 1999: Improved application of exponential sum fitting transmissions to inhomogeneous atmosphere. *J. Geophys. Res.,* **104** (D6), 6291–6303.

——, and D. Pethick, 2002: Comparison between observed and modeled radiative properties of stratocumulus clouds. *Quart. J. Roy. Meteor. Soc.,* **128,** 2691–2712.

Tiedtke, M., 1989: A comprehensive mass flux scheme for cumulus parameterization in large-scale models. *Mon. Wea. Rev.,* **117,** 1779–1800.

Tomas, R. A., and P. J. Webster, 1997: The role of inertial instability in determining the location and strength of near-equatorial convection. *Quart. J. Roy. Meteor. Soc.,* **123,** 1445–1482.

Trenberth, K. E., D. P. Stepaniak, and J. M. Caron, 2000: The global monsoon as seen through the divergent atmospheric circulation. *J. Climate,* **13,** 3969–3993.

Wang, B., and Y. Wang, 1999: Dynamics of the ITCZ-equatorial cold tongue complex and causes of the latitudinal climate asymmetry. *J. Climate,* **12,** 1830–1847.

Wang, Y., 1996: On the forward-in-time upstream advection scheme for non-uniform and time-dependent flow. *Meteor. Atmos. Phys.,* **61,** 27–38.

——, 1999: A triply nested movable mesh tropical cyclone model with explicit cloud microphysics—TCM3. BMRC Research Rep. 74, Bureau of Meteorology Research Centre, Australia, 81 pp.

——, 2001: An explicit simulation of tropical cyclones with a triply nested movable mesh primitive equation model: TCM3. Part I: Model description and control experiment. *Mon. Wea. Rev.,* **129,** 1370–1394.

——, 2002: An explicit simulation of tropical cyclones with a triply nested movable mesh primitive equation model: TCM3. Part II: Model refinements and sensitivity to cloud microphysics parameterization. *Mon. Wea. Rev.,* **130,** 3022–3036.

——, O. L. Sen, and B. Wang, 2003: A highly resolved regional climate model (IPRC–RegCM) and its simulation of the 1998 severe precipitation events over China. Part I: Model description and verification of simulation. *J. Climate,* **16,** 1721–1738.

——, S.-P. Xie, H. Xu, and B. Wang, 2004a: Regional model simulations of boundary layer clouds over the southeast Pacific off South America. Part I: Control experiment. *Mon. Wea. Rev.,* **132,** 275–296.

——, H. Xu, and S.-P. Xie, 2004b: Regional model simulations of boundary layer clouds over the southeast Pacific off South America. Part II: Sensitivity experiments. *Mon. Wea. Rev.,* **132,** 2650–2668.

Wyant, M. C., C. S. Bretherton, H. A. Rand, and D. E. Stevens, 1997: Numerical simulations and a conceptual model of the subtropical marine stratocumulus to trade cumulus transition. *J. Atmos. Sci.,* **54,** 168–192.

Xie, S.-P., 1996: Westward propagation of latitudinal asymmetry

in a coupled ocean–atmosphere model. *J. Atmos. Sci.,* **53,** 3236–3250.

——, and S. G. H. Philander, 1994: A coupled ocean-atmosphere model of relevance to the ITCZ in the eastern Pacific. *Tellus,* **46A,** 340–350.

——, and K. Saito, 2001: Formation and variability of a northerly ITCZ in a hybrid coupled AGCM: Continental forcing and oceanic–atmospheric feedback. *J. Climate,* **14,** 1262–1276.

Xu, H., Y. Wang, and S.-P. Xie, 2004: Effects of the Andes on eastern Pacific climate: A regional atmospheric model study. *J. Climate,* **17,** 589–602.

Xu, K.-M., and D. A. Randall, 1996: A semiempirical cloudiness parameterization for use in climate models. *J. Atmos. Sci.,* **53,** 3084–3102.

Yu, J.-Y., and C. R. Mechoso, 1999: Links between annual variations of Peruvian stratocumulus clouds and of SST in the eastern equatorial Pacific. *J. Climate,* **12,** 3305–3318.

Yuter, S. E., Y. Serra, and R. A. Houze Jr., 2000: The 1997 Pan American Climate Studies Tropical Eastern Pacific Process Study. Part II: Stratocumulus region. *Bull. Amer. Meteor. Soc.,* **81,** 483–490.

Zhang, C., M. McGauley, and N. A. Bond, 2004: Shallow meridional circulation in the tropical eastern Pacific. *J. Climate,* **17,** 133–139.